

# First comparisons between RINGSS and MASS-DIMM at Tololo

Authors: *A. Tokovinin, E. Bustos, R. Rivera*

Version: 2

Date: 2022-05-13

File: prj/atm/smass/test-may22/RINGSS-May2022.tex



Figure 1: RINGSS system deployed provisionally at Tololo on the ground level in April 2022.

# 1 Deployment and operation

The RINGSS turbulence monitor is developed for testing new sites and for upgrading current MASS-DIMM monitors. The method is described in [1]. The system was deployed at Cerro Tololo for first on-sky tests in October 2021 (see the presentation [2]) without enclosure. The cylindrical enclosure and its control were finished in March 2022, and after testing in the office the system was moved to Tololo on April 25, 2022. As for the first tests, it was installed on the ground level for easy access and tuning (Fig. 1). After this initial testing period, RINGSS will be mounted atop the empty Halfmann tower and operated as regular site monitor. The data collected during the first week of RINGSS operation look encouraging, while being still preliminary. Their analysis is presented below.

RINGSS was operated semi-automatically while developing and tuning the control software, `director.py`, that connects to other system components (enclosure, mount, camera) and orchestrates the operation. Stars are selected from a fixed list, pointed and changed at fixed sidereal time. Stars are always pointed east of the meridian. Tracking can continue for up to 2 hours past the meridian. We wanted to avoid the meridian flips which are programmed in the mount control. However, pointing the same star after meridian (e.g. for pointing correction or after cloud passage) causes the mount flip. On the first night (Apr 25), the pointing model of the mount was determined using the hand paddle control, after an initial coarse adjustment of the polar axis. Despite the large residual errors of the polar alignment ( $-3.64$  and  $+3.3$  degrees), the model works well and the stars are always found in the wide (1024 pixels) field of the main camera. Now the flips are accounted for in the centering and guiding algorithms by changing the sign of the RA correction past the meridian.

Upon pointing the star, the wide-field image (snapshot) is taken and the star is centered in two iterations (the mount is pointed to an updated position). Then series of 10 data cubes are taken. Each cube has dimension of  $64 \times 64 \times 2000$ , takes 2s (exposure time 1 ms per frame) and occupies 16 MB of the disk space. Each cube is processed after acquisition using python software. The image parameters (center coordinates and ring radius) are used for guiding and focus control in closed loop. The parameters and statistical moments of each cube are saved as one line in the `.stm` text file. Each line begins with the tag 'm', followed by the date-time stamp and the star HR number. Average parameters of 10 consecutive cubes are saved in the same file with the tag 'M' and the number of averaged cubes, 10. In steady operation, each 10-cube series (including image processing and guiding) takes 53s, or 5.3s per data cube on average.

# 2 Validation of the `.stm` data

During first nights, while the operational algorithm was developed, individual data cubes were recorder and later copied and processed with the IDL software. Starting from Apr 29, the `.stm` text files became reliable. During 6 h of operation on that night, a total of 2566 data cubes were recorded. This material is used to compare the python and IDL processing of individual data cubes, reported in this section. Several `.stm` files recorded on that night were concatenated into a single file and ingested in the data structure using the IDL code `allstm.pro`. Individual (m-tag) lines were ingested. The data were processed by the same code as used for the IDL-processed cubes, and the two resulting data structures of the same format could be compared. However, the numbers of records in these structures (after filtering each to remove large guiding errors or other glitches) are not the same (2479 in `stm` and 2060 in IDL). The time derived in IDL from the data-cube name (e.g. `2022-04-29-225906_cube`) differs by

2s from the time stamp in the .stm file (2022-04-29-22:59:08).

Originally, the IDL processing gave smaller residuals compared to the same .stm data. This was traced to the fact that the flux in .stm is written in ADU, while in IDL it is converted to electrons (0.36 el/ADU for camera gain of 200). As a result, the photon-noise was under-estimated, the large- $m$  moments were biased, and the ground layer was over-estimated. Attempts to fix the issue by reducing the maximum term used for profile restoration (from  $m=17$  to 15 or even 12) or by changing the nominal layers were fruitless until the bug was discovered and fixed.

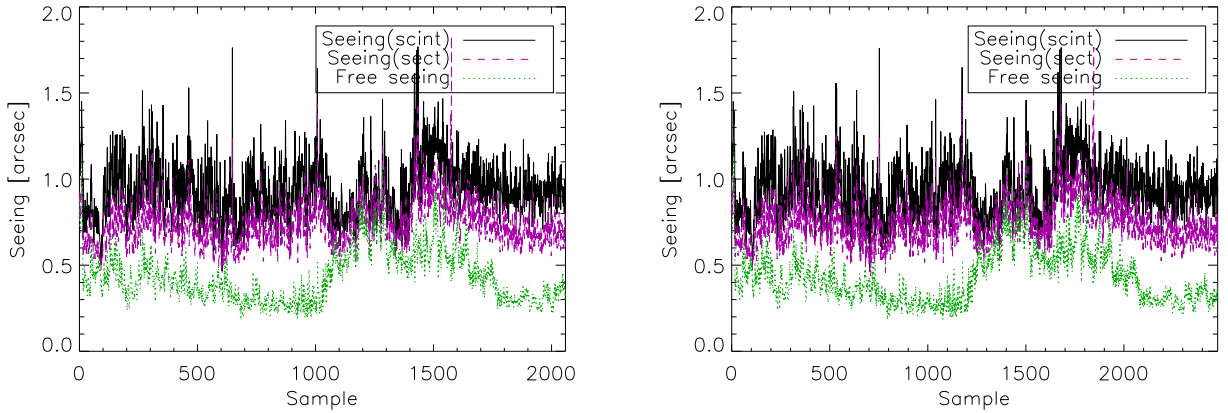


Figure 2: Plots of the seeing vs. sample number for the night of April 29, 2022. Left: IDL processing, right: .stm processing.

Figure 2 shows the results of processing individual data cubes either fully with IDL or by using the statistical moments from .stm. Apart from the slightly different number of samples, the results are now identical. Detailed comparison of seeing plotted vs. time shows that the results are same (apart from the 2-s time shift mentioned above).

The Figure also shows that the seeing computed from the differential sector motion (magenta dashed line) is systematically smaller than the seeing computed from scintillation (solid black line). This effect was noted on all other nights; the mean ratio of two seeings was 0.80. The reason is an incorrect pixel scale of  $1.41''$  used in the data interpretation. It was based on the measurements in March 2021, but earlier measurements in January 2021 indicated  $1.75''$ . The pixel scale was accurately measured by taking snapshot images of 4 wide double stars on May 5, 2022. The result is  $1.78 \pm 0.1$  arcsec. The scale is very sensitive to the distance between the lens and the CCD, so it should be measured for each RINGSS instrument.

The modified pixel size changes the conjugation height (computed from the ring radius in pixels) and the weighting functions (WFs) used for turbulence profile restoration. The WFs are also affected by static aberration. The coma aberration of 0.09-0.12 (in internal dimensionless units, about 1 rad rms) is consistently estimated by the cube-processing software and evident in the average ring images (the upper part of the ring is brighter). The WFs were computed by setting the coma amplitude to 0.12. They are plotted in Fig. 3, left, for a blue star (the WFs are interpolated using the  $B - V$  star color). The right panel shows the same WFs computed earlier with inaccurate pixel scale. Both sets of WFs look qualitatively similar, but differ numerically at large  $m$  and at small distance  $z$ . The

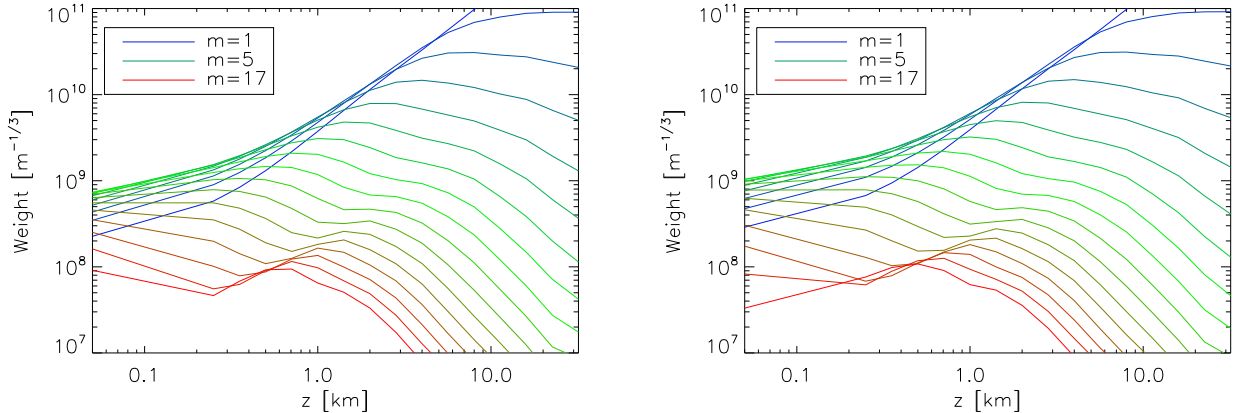


Figure 3: Weighting functions of RINGSS at Tololo for a star of  $B - V = 0$  and coma coefficient of 0.12. Left: with correct conjugation of 440 m, right: wrong conjugation of 540 m.

telescope was better aligned on May 5, reducing the coma amplitude to 0.045.

After fixing the pixel scale and computing the correct WFs, the turbulence profiles were determined from the 10-s average moments recovered from the same .stm files (lines with tag 'M'). The results are less noisy, as evidenced by comparing Figs. 4 and 2. Now the two independent seeing estimates (from scintillation and sector motion) agree very well. The quality of the data fits (rms relative discrepancy between data and model) has improved after the pixel-scale correction and is typically less than 0.1. On April 29 the flux was unstable because of cirrus clouds, but this had no effect on the data quality.

The initial processing of the data with inaccurate pixel scale and with under-subtracted photon noise returned results that are also inaccurate, but not too wrong either. The RINGSS method is relatively robust. Furthermore, the two internal quality metrics (the rms residual error and the agreement between two independent seeing estimates) readily detect problems.

### 3 First comparison with Tololo MASS-DIMM

Data from the Tololo MASS-DIMM seeing monitor were recovered from the web site<sup>1</sup> and ingested in IDL. For each RINGSS measurement, the MASS-DIMM data matching in time within 1 min. were found and averaged. For this comparison, the free-atmosphere (FA) seeing in RINGSS is computed from the sum of all integrals at 0.5 km and above, adding half of the integral at 0.25 km to account for MASS partial sensitivity at this height.

Figure 5 shows the XY comparison plots of the full and FA seeing on two nights. It is expected that RINGSS, installed at a lower height above ground, could be affected by additional turbulence and measure a larger seeing. So far, this is not observed and, on the contrary, on May 1 RINGSS recorded a slightly better seeing than DIMM. It looks like MASS is measuring a larger FA seeing than RINGSS, even after adding part of the 0.25-km layer. This is more visible in the layer-by-layer comparison between RINGSS and MASS profiles shown in Fig. 6. Qualitatively, both instruments detect transient

<sup>1</sup>[http://139.229.13.222/web/CTIO/massdimm\\_data\\_plot.php](http://139.229.13.222/web/CTIO/massdimm_data_plot.php)

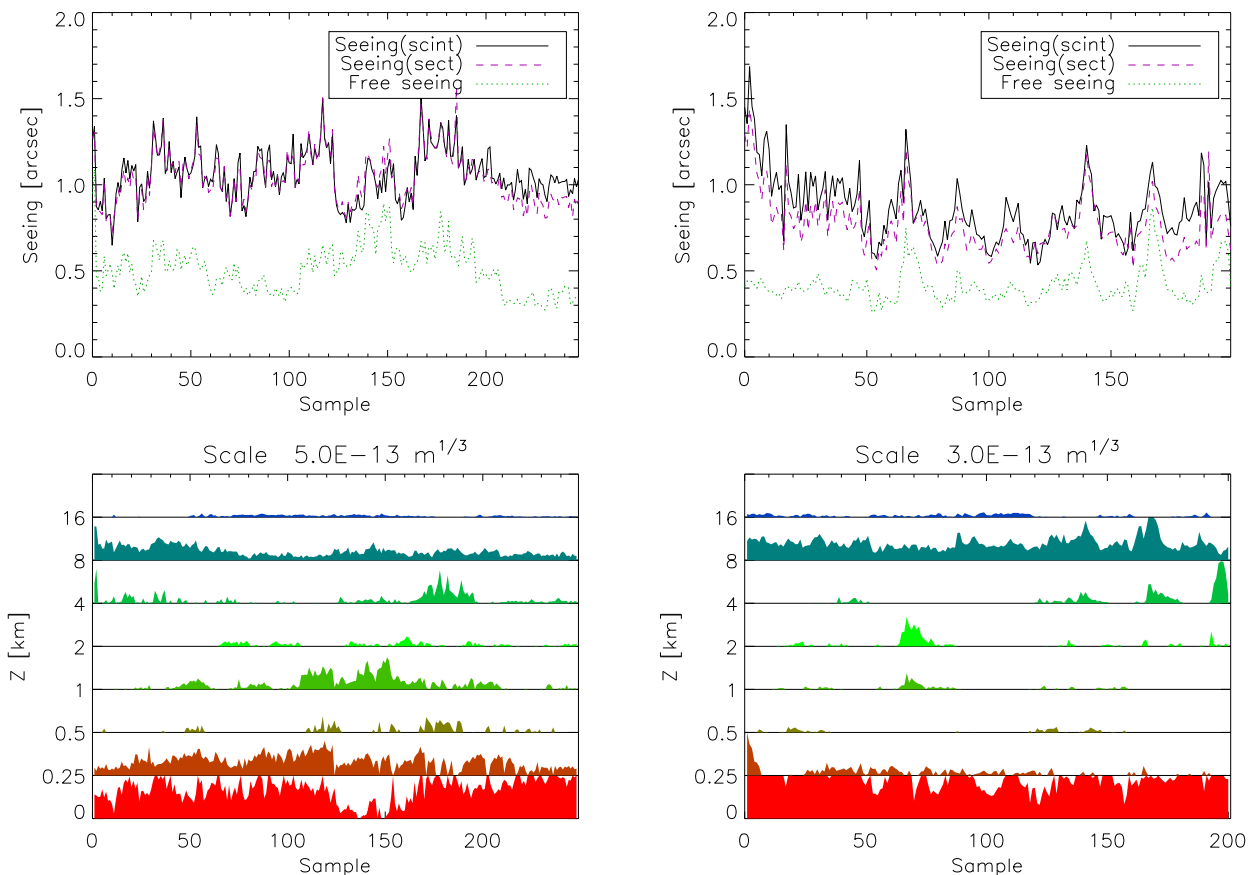


Figure 4: Seeing plots for April 29 (left) and May 1 (right) derived from the 10-s average moments with corrected pixel scale and WFs. The lower panels show turbulence profiles (the  $C_n^2 dh$  scale corresponding to one interval is indicated in each plot).

packets of turbulence in the high atmosphere, but the distribution of this turbulence between the layers is not the same. The two instruments looked at different stars, so detailed correlation in time is not expected (they look through turbulent 'clouds' at different time). MASS systematically measures a stronger turbulence at 0.5 km and a weaker turbulence at 8 km. Note that on April 29 MASS could be adversely affected by cirrus clouds.

The night of May 2 was remarkable by its poor seeing (between  $2''$  and  $3''$ ) caused primarily by the high-altitude turbulence. Strong scintillation puts RINGSS near the limit of its operating range (its theory is based on the weak scintillation assumption with empirical corrections). Still, the two seeing estimates remain in reasonable mutual agreement and the RINGSS seeing agrees with DIMM or is slightly larger, as expected from the larger ground-layer contribution (Fig. 7).

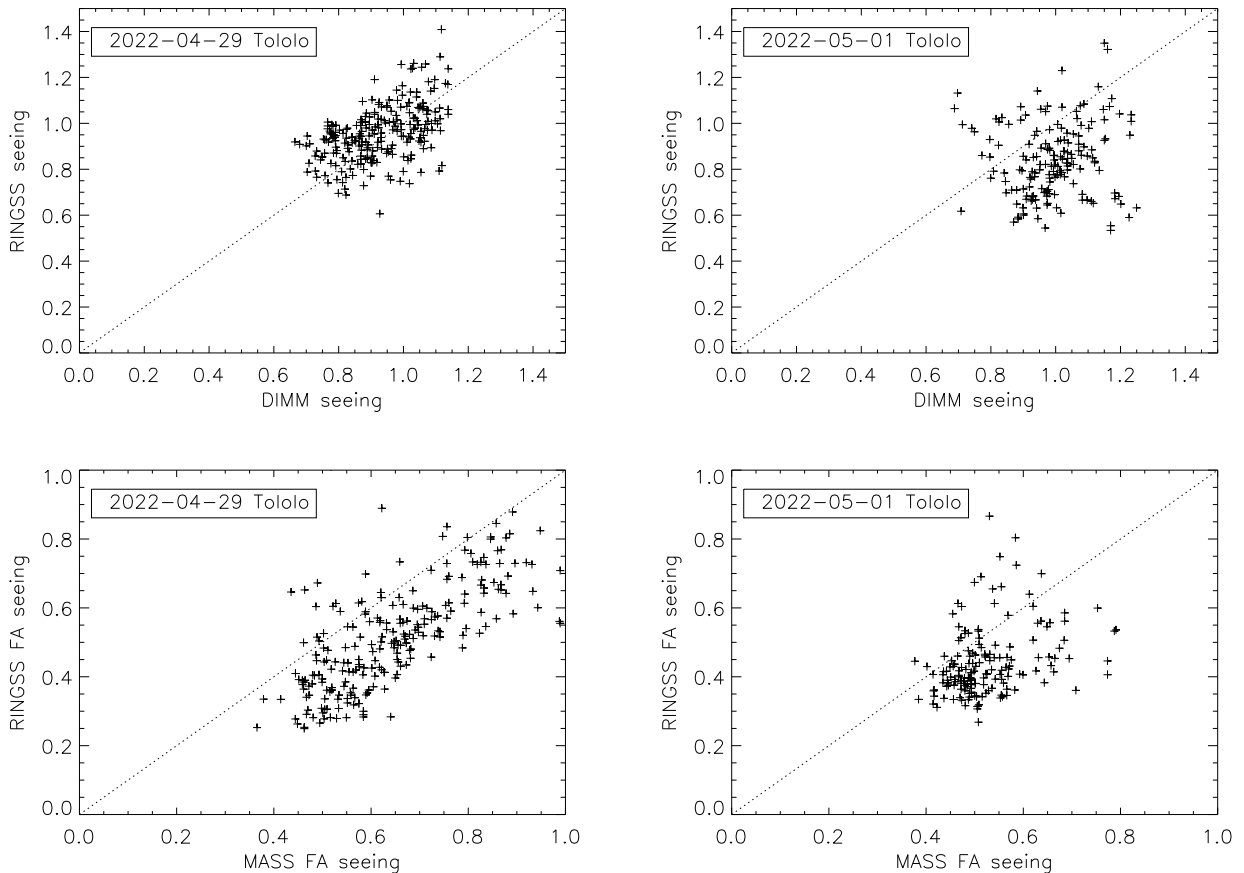


Figure 5: Comparison between RINGSS and MASS-DIMM on April 29 (left) and May 1 (right). The top plots show the total seeing, the lower plots – the free-atmosphere seeing. The dotted line corresponds to equality.

## 4 A night with good seeing

On the night of May 11/12, RINGSS operated robotically for 9 hours and the seeing was good, with minor cirrus passages at times. This night tests the RINGSS operation under good seeing.

Figure 8 presents the internal RINGSS seeing plot and the turbulence profiles on May 11/12 2022. We note that the sector seeing is at times slightly larger than the scintillation seeing; their average ratio is 1.08. This ratio does not show any correlation with the rms error of profile restoration, wind, FA seeing, or flux (the latter tests the correctness of the noise-bias subtraction). However, it shows an anti-correlation with the first (ground) layer turbulence, suggesting that scintillation can slightly under-estimate this layer. Figure 9 (left) compares the RINGSS seeing (scintillation) with the DIMM seeing. The average ratio is close to one, but it varies with time. Up to 4 h UT, RINGSS measured a better seeing than DIMM, despite its lower altitude above ground. After that, RINGSS measured seeing spikes caused by the strong near-ground turbulence. The right-hand plot shows a

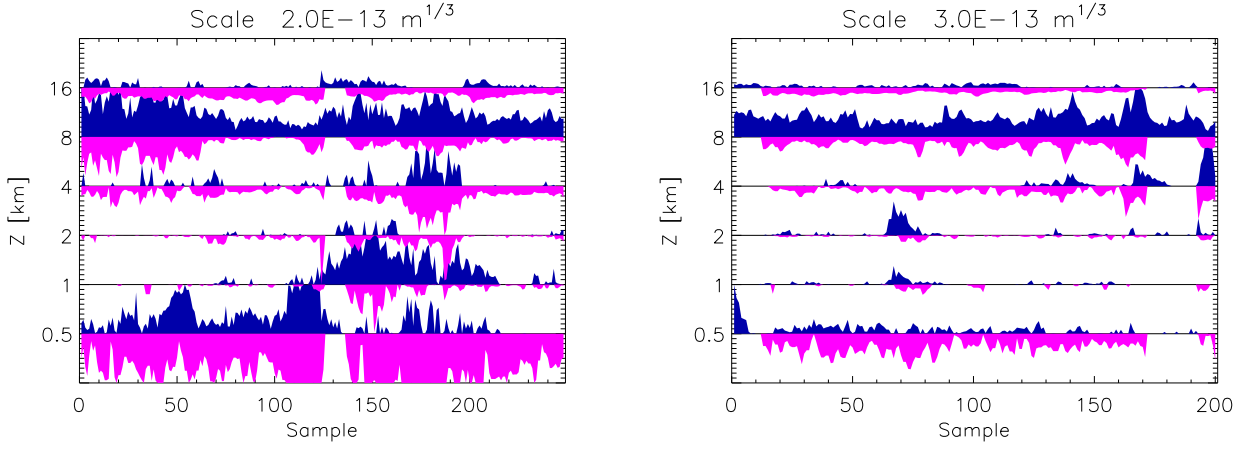


Figure 6: Comparison between RINGSS and MASS turbulence profiles on April 29 (left) and May 1 (right). The RINGSS turbulence integrals are blue top-facing bars, the corresponding MASS integrals are magenta down-facing bars.

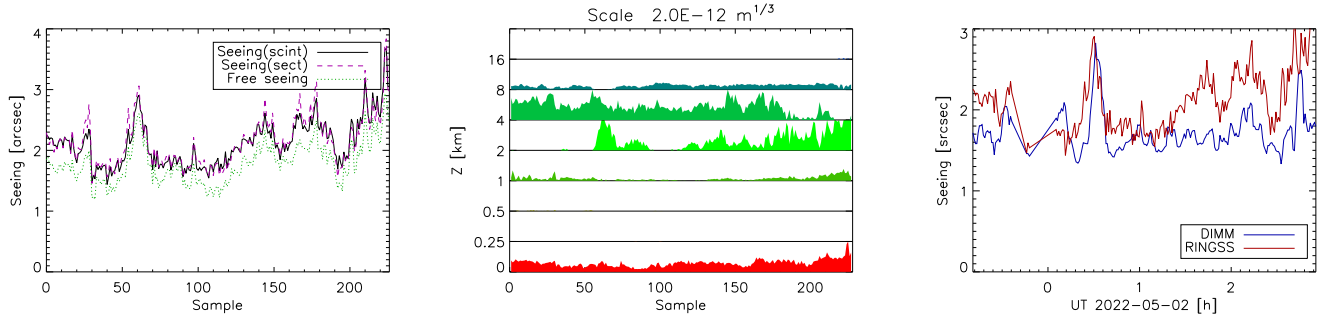


Figure 7: The poor-seeing night of May 2, 2022. The right plot shows seeing vs. time measured by RINGSS and DIMM.

clear correlation of the seeing ratio with the intensity of the ground layer, confirming that the seeing spikes in RINGSS originate near the ground. On the other hand, with a very weak ground layer RINGSS measured a better (half-arcsecond) seeing than DIMM, suggesting that DIMM could be slightly affected by some internal turbulence. This comparison does not change if we use the RINGSS sector seeing instead of the scintillation seeing.

Figure 10, left, compares the FA seeing between RINGSS (all layers from 0.5 km up plus half of the 0.25-km layer) and MASS. The right-hand panel shows the detailed comparison between turbulence profiles. One notes that MASS measured a stronger turbulence at 0.5 km at the beginning of the night and also a somewhat stronger turbulence in the 16-km layer (as on the previous nights), while RINGSS gives a stronger 8-km layer. The qualitative agreement is good, showing similar spikes of turbulence in various layers.

Figure 11 plots the atmospheric time constant  $\tau_0$ . It is computed in RINGSS as  $\tau_0 = 0.31r_0/V$ , where  $r_0$  is the Fried parameter at 500 nm wavelength in the free atmosphere (layers 0.5 km and

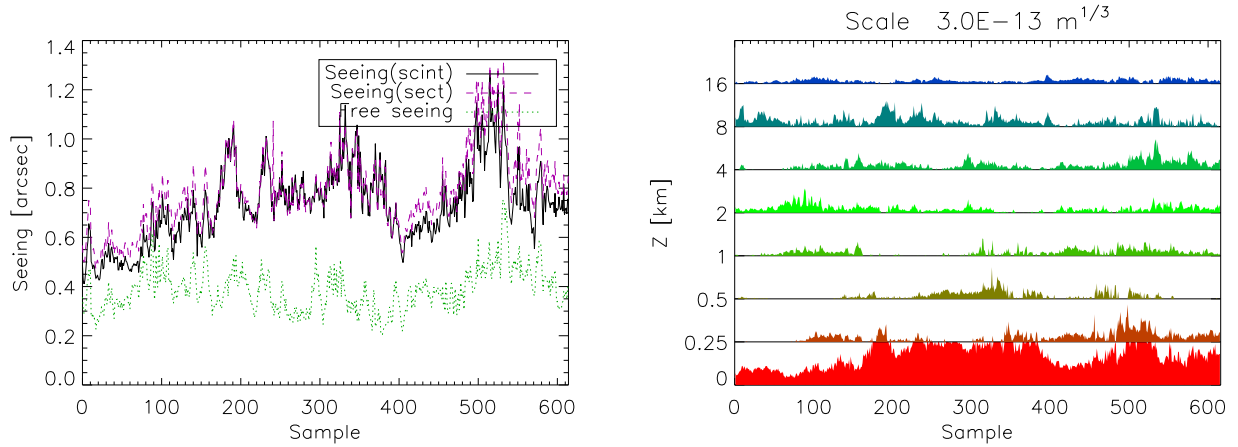


Figure 8: Good seeing on May 11/12, 2022. Left: internal RINGSS seeing plot, right: turbulence profiles.

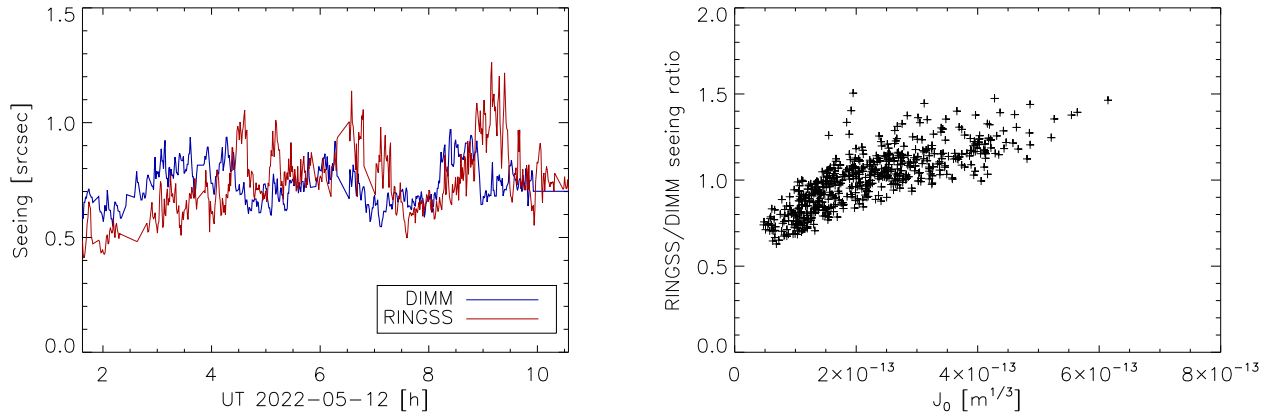


Figure 9: Comparison of seeing measured by RINGSS (scintillation) and DIMM on May 11/12, 2022. Left: seeing vs. time, right: correlation of the seeing ratio with the turbulence integral in the ground layer  $J_0$ . The RINGSS scintillation seeing is used, but the sector seeing shows a similar correlation.

higher) and  $V$  is the effective wind speed delivered by RINGSS. The MASS software estimated  $\tau_0$  by an approximate method and these estimates are increased here 1.4 times, in agreement with previous studies of the  $\tau_0$  bias in MASS [3]. With this correction, the agreement between both instruments is as good as can be expected.

## 5 Preliminary conclusions

The first results of RINGSS test operation at Tololo are encouraging. The on-line processing of the data cubes is fully validated: the .stm files contain all essential information and now the cubes are

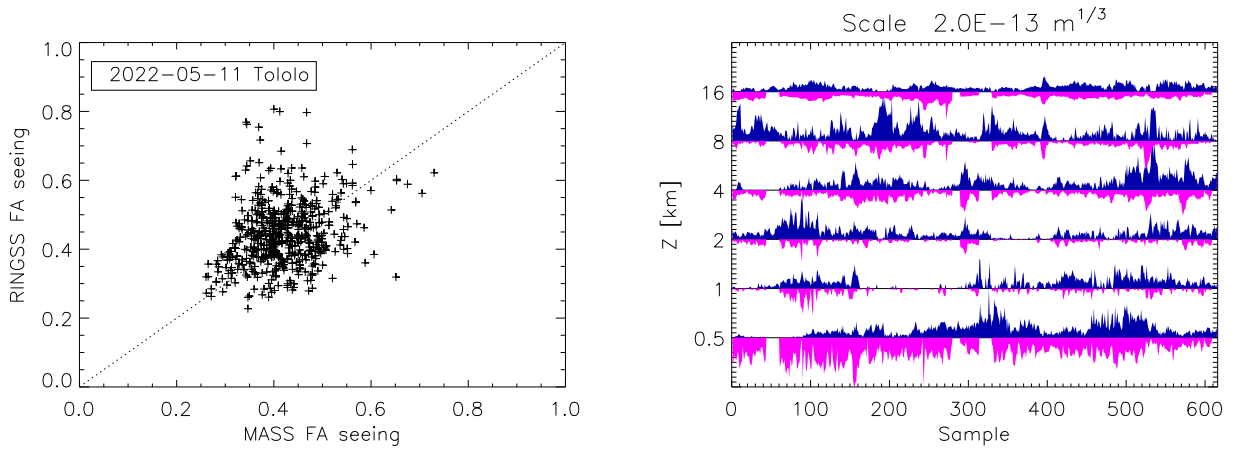


Figure 10: Comparison of FA seeing measured by RINGSS and MASS (left) and comparison of turbulence profiles, similar to Fig. 6.

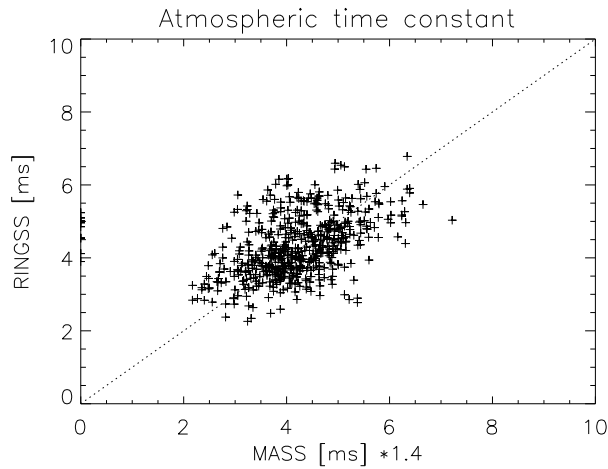


Figure 11: Comparison between atmospheric time constants measured by RINGSS and MASS on May 11/12, 2022.

discarded (not saved). The internal quality control in RINGSS helped to detect and fix problems in the initial data reduction. The data collected so far indicate a reasonable agreement with MASS-DIMM under a variety of conditions, from good to poor.

## References

- [1] Tokovinin A. Measurement of turbulence profile from defocused ring images. 2021, MNRAS, 502, 794-808

- [2] Tokovinin, A. Monitor de turbulencia RINGSS (el hijo de MASS y DIMM). Presentation at CTIO Nov. 23, 2021. <http://www.ctio.noirlab.edu/~atokovin/profiler/RINGSS-CTIO.pdf>
- [3] Tokovinin A. Atmospheric time constant with MASS and FADE. 2010, Kislovodsk conference; ArXiv: 1101.3211. <http://arxiv.org/abs/1101.3211>